Journal of Alloys and Compounds 575 (2013) 198–206

Contents lists available at SciVerse ScienceDirect

Journal of Alloys and Compounds

journal homepage: www.elsevier.com/locate/jalcom

Electrical transport, microstructure and optical properties of Cr-doped In_2O_3 thin film prepared by sol–gel method

H. Baqiah [a], N.B. Ibrahim [a,*], M.H. Abdi [a], S.A. Halim [b]

[a] School of Applied Physics, Faculty of Science and Technology, Universiti Kebangsaan Malaysia, 43600 Bangi, Selangor, Malaysia
[b] Superconductors and Thin Film Laboratory, Department of Physics, Faculty of Science, University Putra Malaysia, 43400 UPM Serdang, Selangor, Malaysia

ARTICLE INFO

Article history:
Received 18 February 2013
Received in revised form 12 April 2013
Accepted 12 April 2013
Available online 22 April 2013

Keywords:
Sol–gel
Indium oxide
Transmittance
Porosity
Conducting mechanism
Hopping conductivity models

ABSTRACT

High transparent In_2O_3 and Cr-doped In_2O_3 ($In_{2-x}Cr_xO_3$) nanocrystalline thin films were prepared using a simple sol–gel method followed by a spin coating technique. The effect of Cr concentration on the structural, microstructure, electrical and optical properties of $In_{2-x}Cr_xO_3$ were systematically investigated using X-ray diffractometer (XRD), atomic force microscopy (AFM), UV–vis spectroscopy, field emission scanning electron microscopy (FESEM) and Hall effect technique. The films have good crystallization with preferred orientation to (222) direction. The lattice parameters, a, of In_2O_3 system increased at lowest dopants ($x = 0.025$) and decreased as the dopant was further increased. The optical transmittance of films increased up to 98% for $x = 0.05$ and decreased for further Cr concentrations. From AFM measurement the films nanocrystals morphology was depending on Cr concentrations. The band gap was around 3.76 eV for pure and with $x \leqslant 0.075$ however it increased. The effect of Cr concentrations on conducting mechanisms of In_2O_3 film has been investigated from 80 to 300 K using thermal activated conduction band and hopping models. The films, at $x = 0.0$–0.075, have typical semiconductor behaviour. Three different conducting mechanisms have been estimated. All thermal activation energies and conduction hopping parameters have been determined and analysed in details.

1. Introduction

Transparent semiconductor oxides (TCOs) are transparent materials with good electrical conductivity. It has been used for many applications such as flat-panel displays, solar cells and gas sensors. Several types of dopants have been introduced into the semiconductor structures in order to make them suitable for certain applications. Many researchers have studied the effect of dopant concentrations on the microstructure, electrical, optical transmission and magnetic properties of TCO in order to improve the material properties [1–6]. The function of dopant is to tune microstructure, transmission and electrical conductivity [1–12] of the semiconductor materials.

Indium(III) oxide (In_2O_3) is one of the (TCO) with a wide band gap value i.e. 3.6 eV. Its electrical and physical properties could also be improved by a doping process. It has been reported that doping In_2O_3 with Sn improves its electrical property making it suitable as an electrode in solar cells, photovoltaics and flat-panel displays [8,9,13,14]. High transmittance (90%) at near-infrared region has been achieved by doping W in In_2O_3 [7].

Cr doped indium oxide has received great attention [15–18] since it has been reported as a possible candidate for dilute magnetic semiconductors [19]. Some researchers have been focused on the structural, optical and electrical properties of Cr doped In_2O_3 thin film_which could give an explanation for possible magnetic properties [20,21]. Hsu studied the crystalline structural transition effect on the electronic-band structure of chromium-doped indium oxide prepared on different substrate Si and yttria-stabilized zirconia (YSZ) substrates by a rf sputtering at room temperature. The growth condition and different type of substrate used, can produce Cr doped In_2O_3 thin films with a different band gap value. It was also reported that the transmission, band gap and electrical properties of laser ablated Cr doped In_2O_3 thin films are dependent on different oxygen pressure during the preparation process [21]. A sol–gel method is a simple and low price method. It also offers precise control of material composition [22–24]. In this paper we report the effect of Cr concentration on structure, microstructure, electrical transport and optical properties of Cr doped In_2O_3 thin film. The details of the conducting mechanism of pure and Cr doped In_2O_3 system were also discussed. It was found that the microstructure, optical and conducting mechanism of indium oxide is highly dependent on the doping concentration of Chromium.

* Corresponding author.
E-mail address: baayah@ukm.my (N.B. Ibrahim).

0925-8388/$ - see front matter © 2013 Elsevier B.V. All rights reserved.
http://dx.doi.org/10.1016/j.jallcom.2013.04.089

2. Experimental

Indium nitrate hydrated $In(NO_3)\cdot H_2O$ and chromium chloride hexahydrate $CrCl_3\cdot 6(H_2O)$ were used as source materials of In^{+3} and Cr^{+3} for the preparation of $In_{2-x}Cr_xO_3$ thin films. Absolute ethanol and acetylacetone were used as solvents. To get a sol, $In(NO_3)\cdot H_2O$ was firstly dissolved in mixture of absolute ethanol and acetylacetone and $CrCl_3\cdot 6(H_2O)$ was dissolved in absolute ethanol. Then each solution was stirred for 1 h at room temperature (30 °C). The solutions were then mixed and stirred for 2 h then it was filtered using 0.45 μm syringe filter and aged for 2 d. Then the aged solution was dropped onto a cleaned soda lime glass substrate and spins coated at 1500 rpm for 30 s. The coated layer was dried at 70 °C for 20 min to evaporate the organic solvent, followed by an annealing process at 500 °C for 30 min. The phase and crystal structure were investigated using a Bruker X-ray diffractometer (XRD) (2θ from 15° to 60°). The surface morphology and roughness were studied using a Nova atomic force microscope (AFM). The optical properties of the films were characterized using a Perkin Elmer (Lamda35) UV–vis spectrophotometer. The Hall Effect measurement was done using a Keithley 2700 multimeter and a Keithley sourcemeter by a Van der Pauw method.

3. Results and discussion

3.1. Microstructure analysis using X-ray diffractometer

Fig. 1 shows the X-ray diffraction patterns of $In_{2-x}Cr_xO_3$ with $x = (0–0.15)$. All observed peaks belong to bixibyte cubic structure with a space group of Ia-3 (206). There is no peak related to chromium oxide or its compound can be observed. The samples have polycrystalline structures with preferred orientation to (222) direction. In order to elucidate the effect of Cr doping in the unit cell of indium oxide, all XRD patterns have been analysed using an EVA software. The XRD patterns of all samples match with JCPDS card number 006-0416 for bulk indium oxide. The lattice parameter for pure sample is 10.108 Å, which is less than the value for standard bulk In_2O_3 (10.118 Å). The lattice parameters of all samples are summarized in Table 1. The effect of Cr concentration ranged from $x = 0.025$ (1.25%) to $x = 0.15$ (7.5%) on the unit cell of indium oxide can be divided to two effects. For low doping where there isn't enough Cr^{3+} ion to replace indium site, Cr^{3+} sits at an interstitial site in unit cell instead, resulting in a small expansion of a lattice parameter a. This phenomena is possible because the ionic radius of Cr^{3+} ion ($R_{Cr} = 0.61$ Å) is smaller than the ionic radius of In^{3+} ($R_{In} = 0.80$ Å) and In_2O_3 has a bixibyte unit cell consists of 32 In atoms and 48 oxygen atoms. A similar result has been reported for Sn doped In_2O_3 [25–27]. For higher dopants $x > 0.025$ (1.25%) the lattice parameter, a was monotonically decreased by increasing Cr concentration. The inset in Fig. 1 shows (222) plane shifts to lower angle for sample with low doping $x = 0.025$ (1.25%) and shifts to higher angle with $x > 0.025$.

The crystallite size of all samples was calculated using Scherrer's Eq. (1) followed,

$$D = k\lambda/\beta\cos\theta \quad (1)$$

where D, k, λ, β and θ are the crystalline size, Scherrer constant which is equal to 0.9, the wavelength of Cu Kα radiation ($\lambda = 1.5406$ Å), width at half maximum FWHM in radian and Bragg angle, respectively. The crystallite size calculated from the most intense peak i.e. (222) plane is tabulated in Table 1. All the parameter in Eq. (1) was determined from the analysis of the XRD pattern using the EVA software. The results show that the crystallites sizes are independent from the Cr concentrations.

3.2. Morphology and microstructure analysis

Fig. 2 shows AFM 2D and 3D of images (5 μm × 5 μm) of the thin films. It clearly shows that the morphology of indium oxide affected by chromium concentrations and has a different growth pattern. For samples $x = 0.025$ and $x = 0.05$, the grains have a spherical shape and tend to agglomerate to each other. Sample $x = 0.075$, the surface has spherical particles with better distribution however small pores can be observed on the surface. By increasing the Cr doping, the porosity increases and the spherical shape of grain changes and tend to elongate and form in flowers like shape for $x = 0.15$. The root mean square roughness varied from 1.755 nm for sample $x = 0.025$ to 7 nm for sample with $x = 0.15$ and this variation depends on the grains agglomeration and porosity of the sample's surface as can be noted in Fig. 2.

Fig. 3 shows a typical FESEM cross section micrographs for the sample with $x = 00$ and $x = 0.05$. The films have smooth dense thin layer and consist of small particles. The film also shows good adhesion to glass substrate.

Fig. 4 shows the XPS spectra of elemental composition of sample with $x = 0.05$. The In 3d spectra appear at 444.47 eV and 452.06 eV for In 3d5/2 and In 3d3/2 transition. The Cr 2p spectra appear at 576.83 eV and 586.23 eV for Cr 2p3/2 and Cr 2p1/2 which are related to Cr+3 states for Cr atom. The spectra of O 1s can be split into two peaks at 529.57 eV and 531.18 eV. The first transition belongs to In–O bonding in In2O3 system. The shifting of O 1s

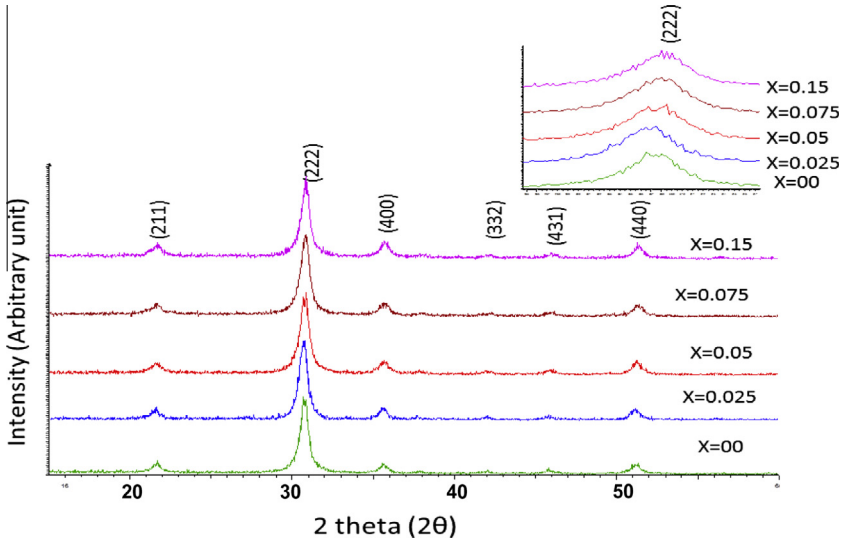

Fig. 1. X-rays diffraction pattern of $In_{2-x}Cr_xO_3$ films with ($x = 0.0–0.15$).

Table 1
Lattice parameter, relative reliability of lattice parameter R/R_0, crystal size, root mean square roughness, film thickness and band gap.

Chromium concentrations	Lattice parameter (Å)	R/R_0	Crystal size (nm)	Root mean square roughness (nm)	Thickness (nm)	Band gap (eV)
$x = 0$	10.108	1.2	12.1	2	93.4	3.76
$x = 0.025$	10.109	1.3	13.3	1.7	87.84	3.75
$x = 0.05$	10.0984	1.2	12	3.2	84.8	3.76
$x = 0.075$	10.0971	1.2	12.6	2.6	104.97	3.76
$x = 0.15$	10.0778	1.3	13	7	100.5	3.79

R/R_0 is the relative reliability of lattice parameter of simulation fitting of XRD pattern. For perfect fitting R/R_0 is 1.

spectra in the second transition could be related to the change of the surrounding oxygen atoms. Oxygen vacancies and Cr dopant have role to determine properties of TCO systems.

3.3. Electrical properties of Cr doped In_2O_3 at room temperature (30 °C)

The electrical properties at room temperature (30 °C) of Cr doped indium oxide thin films are shown in Fig. 5. The resistivity, carrier concentration and mobility of pure indium oxide are 0.29 Ω cm, 1×10^{19} cm^{-3} and 2.1 cm^2 V^{-1} S^{-1} respectively. In earlier reports of In_2O_3 prepared by the sol–gel method followed by multiple-dipping process, the resistivity, carrier concentration and mobility are around 0.6 Ω cm, 2.1×10^{19} cm^{-3} and 0.2 cm^2 - V^{-1} S^{-1} for In_2O_3 thin film annealed twice at 500 °C. First annealing at 500 °C gives the resistivity of 5 Ω cm [28]. Our pure In_2O_3 has lower resistivity and higher mobility compared with the previous report. This is due to the good crystallinity and dense layer of the films (see Figs. 1 and 3). Fig. 5 also shows that the resistivity of all films increases while the carrier concentration decreases gradually with the increment of Cr concentration. Based on the stoichiometry calculation involved during the sample preparation, increasing the Cr dopant will reduce the In. The conductivity of In_2O_3 system is originated from interstitial indium that acts as a shallow donor level near the conduction band. The generation of carrier concentration occurs when interstitial indium and oxygen vacancies exist in the system [29]. Thus increasing the dopant will reduce the carrier concentration and the resistivity will increase. Another factor that could cause the increase of resistivity of films is the porosity that starts to appear at $x = 0.075$ and increases with the increment of Cr. Fig. 5 also shows the effect of Cr concentrations on the mobility of the In_2O_3 thin films. The relation between carrier concentrations (n) and mobility (μ) is given by $\mu = 1/e\rho n$ (ρ is the resistivity and e is the electron charge). This equation clearly indicates why mobility increases while the carrier concentration decreases. Similar results have been reported by [3,30].

3.4. Conducting mechanism at low temperature

The conducting mechanism of pure and Cr-doped indium oxide below room temperature has been studied using thermal activated conduction band and hopping models which are commonly used to describe conducting mechanism in semiconductors [31–34]. Three different conducting regions could be estimated using linear fitting techniques. A minimum fitting coefficient that has been used is more than or equal to 0.99. The conducting mechanism of doped semiconductor could cross over from thermal activated to nearest–nearest neighbor hopping (NNH) to a variable range hopping with decreasing temperature [35]. First, the conductivity at room temperature has been fitted with Eq. (2) in order to check the possibility of thermal activation conduction. Second, conductivity above 80 K has been fitted with hopping conductivity models. The third region has been determined by the mean of best line fit with all previous models as it is further illustrated below.

$$\sigma = \sigma_0 \exp(-E_{a1}/k_B T) \tag{2}$$

Fig. 6 shows an Arrhenius plot of pure and Cr doped indium oxide. All samples show typical semiconductor behavior in the temperature range from 80 K to 300 K. Maximum fitting of Eq. (2) has been found nearly in the range 200–300 K. This indicates the electrical conductivity in this range is dominated by thermal activated conduction band. The temperature range, fitting coefficient R^2 and thermal activated conduction band are shown in Table 2. The thermal activated conduction band of thin films decreases when the Cr doping increases. It is known that the conductivity of pure In_2O_3 is originated from the coexistence of interstitial indium atoms and oxygen vacancy. Interstitial indium acts as a shallow donor while an oxygen vacancy helps the formation of carriers [29]. The doping of Cr may form a deep impurity band in band gap which causes a shallow donor or an oxygen vacancy decreases thus reduces the thermal activation energy, E_a. Similar behavior has been observed in Mn doped Zno thin films [31].

For further investigation of the conductivity mechanism in the range 200–300 K, the effect of grain boundary on the transport properties is evaluated by calculating the Debye screening length for n type semiconductor as follows [36]:

$$L_D = \left(\frac{\varepsilon\varepsilon_0 k_B T}{e^2 N_d}\right)^{1/2} \tag{3}$$

where ε dielectric constant, ε_0 is the dielectric constant of vacuum and N_d is donor concentration from Hall effect measurement. If L_D is smaller than $l/2$, where l is the grain size, there is a potential barrier affects the passing electron across the grain boundary. The calculated L_D is listed in Table 2. The L_D is smaller than $l/2$ which means that the grain boundary scatters the passing electron through it. The conductivity through grain boundary barrier σ_b is described by Eq. (4) [33]:

$$\sigma_b = CT^{-1/2} \exp(-E_b/k_B T) \tag{4}$$

where C is constant and E_b is the activated energy for grain boundary limited conductivity k_B is the Boltzmann constant. The relation between $\ln\sigma_b$ $T^{1/2}$ and $1/T$ has good linearity which confirms the thermionic emission through grain boundary. The E_b has been calculated from the slope line and listed in Table 2.

The second region is determined after region I and region III have been estimated with the benefit of the rule that thermal activated conduction band occurs at high temperature while the variable range hopping conduction occurs at low temperature [35]. The conductivity in region II for samples with $x = 0.0$–0.05 is most suitable to be described with nearest–nearest hopping (NNH). This requirement of variable range hopping isn't fulfilled due to the small value of localize hope length in this region, $\xi < 1$ nm. Also the NNH mechanism occurs at relatively high temperature. The conductivity at high temperature can be generally expressed by Eq. (5). The NNH mechanism in the range 150–200 K was also reported for SnO_2 film prepared by sol–gel spin coated method by [32].

$$\sigma = \sigma_{01} \exp(-E_{a1}/k_B) + \Gamma_{02} exp(-E_{a2}/k_B T) \tag{5}$$

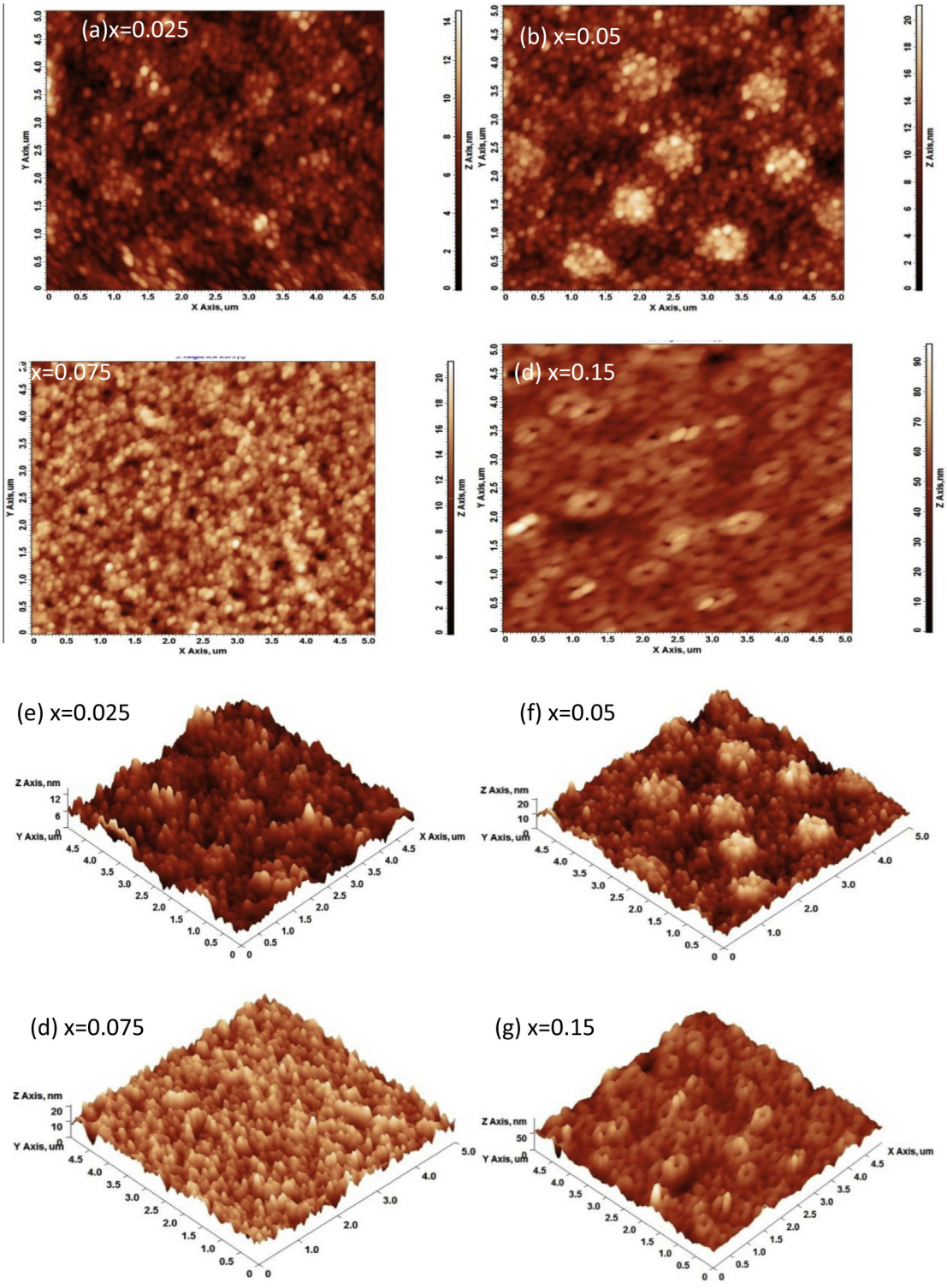

Fig. 2. AFM 2D and 3D images (5 μm × 5 μm) of $In_{2-x}Cr_xO_3$ thin films with x = (00, 0.025, 0.05, 0.075 and 0.15). 2D (above) and 3D (below).

The first part of the equation represents conductivity characterized by thermal activated conduction band and the second part represent conductivity by hopping between nearest–nearest neighbors [35]. The activated energy for NNH hopping is calculated from the second part of Eq. (5). Fig. 7a shows the relation between $\ln\sigma$ and $1/T$ in the range of 130–200 K for samples with x = 0–0.05. The temperature range and fitting coefficient are listed in Table 2. It can be noticed that $E_{a1} > E_{a2}$ because the first one E_{a1} is the thermal excitation of electrons from shallow donor to the conduction band while the E_{a2} is thermal excitation within donor level itself.

At lower temperature the number of free neighbor sites becomes too small and these results in freezing out the NNH hopes which could lead to new hopping mechanism called variable range

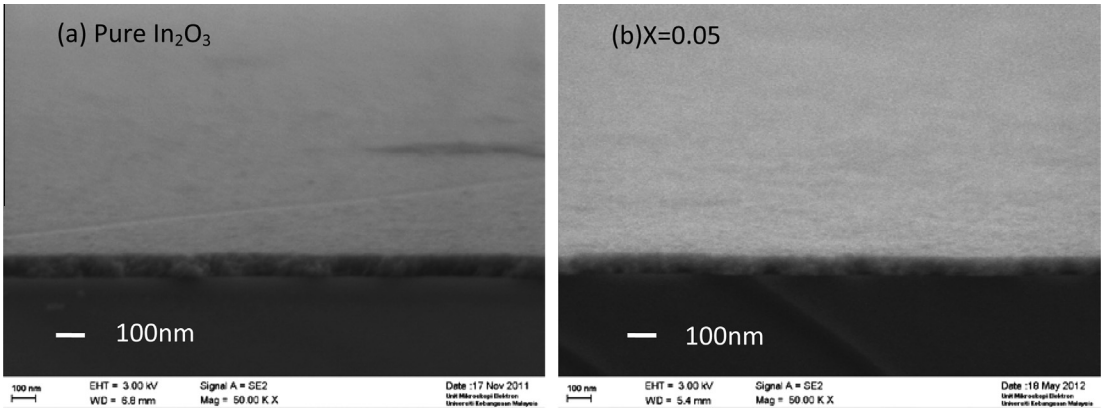

Fig. 3. Cross section of (a) pure In_2O_3 and (b) Cr doped-indium oxide film with $x = 0.05$.

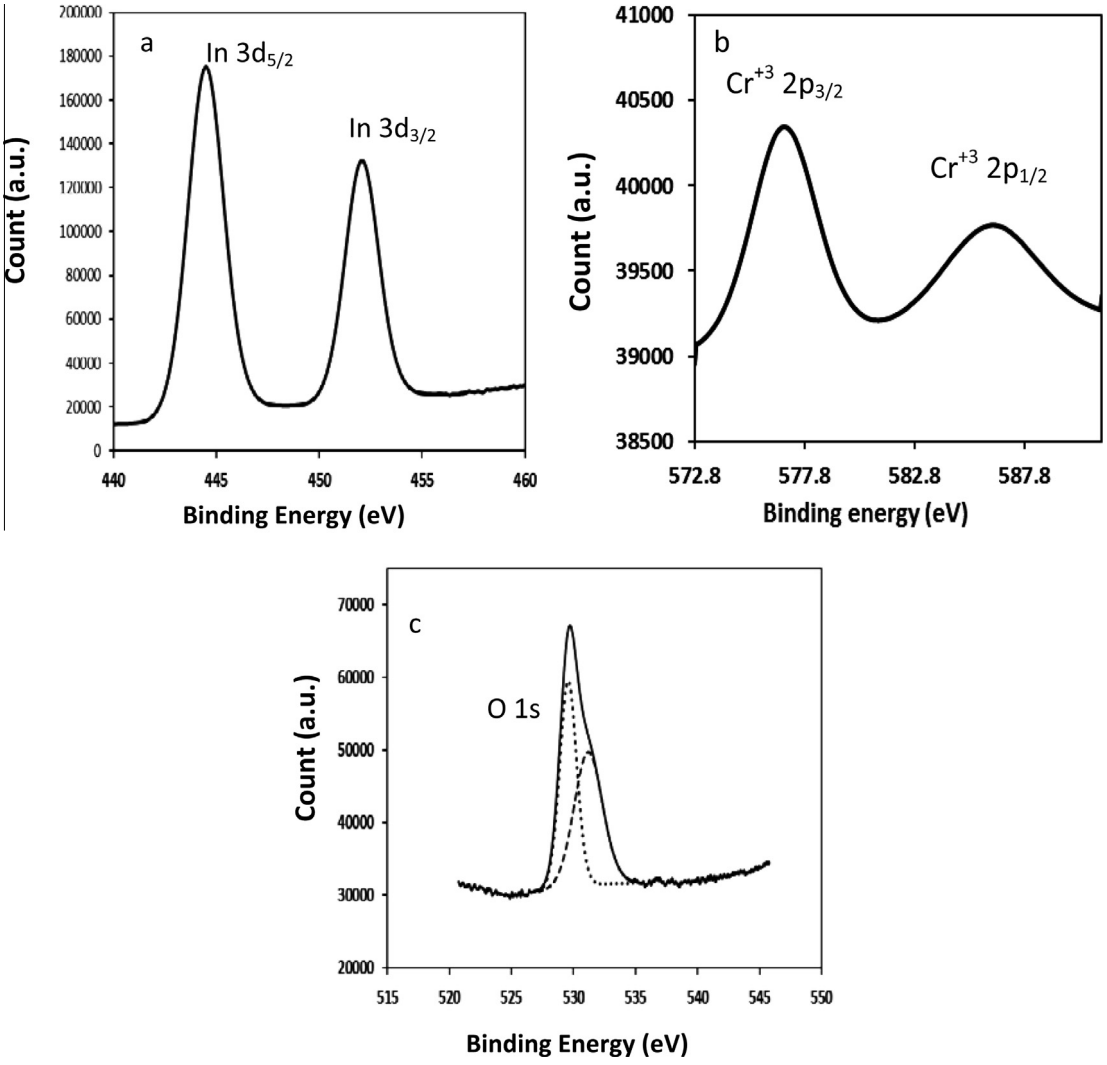

Fig. 4. Typical XPS spectra for the samples: (a) In 3d; (b) Cr 2p at $x = 0.05$ of Cr doped In_2O_3 system and (c) O 1s.

hopping (VRH). The hopping arises between sites in vicinity of Fermi level and it doesn't have a constant distance like nearest–nearest neighbor hopping. If the density state around the Fermi level is constant, there is a possibility to Mott VRH mechanism. On the other hand if there is a gap at the Fermi level due to electron–electron interaction the hopping mechanism is related to Efros–Shklovskii (ES) VRH [35].

The conductivity via Mott VRH mechanism is given by Eq. (6)

$$\sigma_{\text{VRHt Mott}} = \sigma_{0\text{Mott}} T^{-1/2} \exp\left(-T_{0\text{Mott}}/T\right)^{1/q} \quad (6)$$

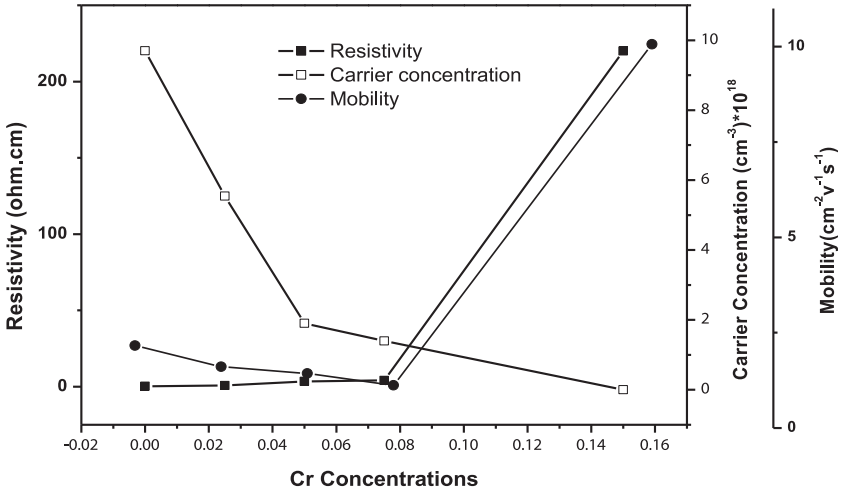

Fig. 5. Resistivity, carrier concentration and mobility against Cr concentration.

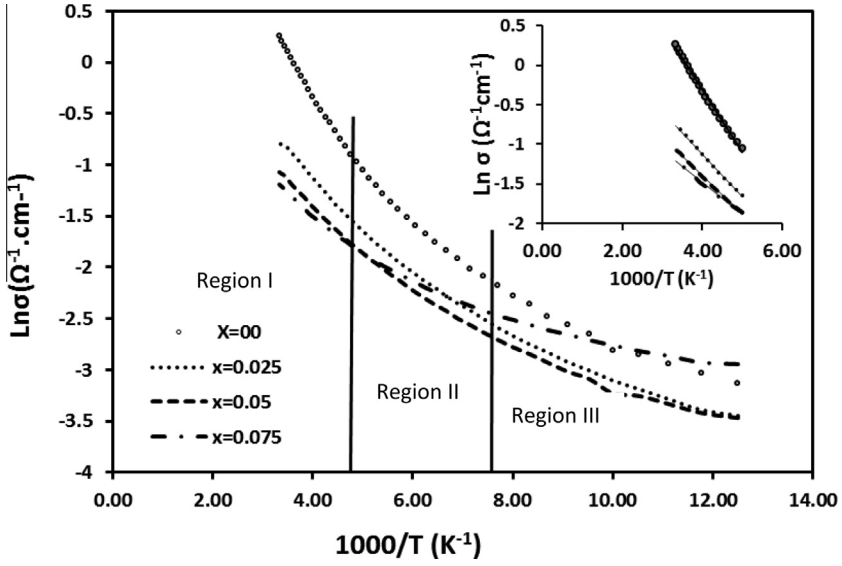

Fig. 6. Arrhenius plot of Cr doped In_2O_3 thin films with $x = 0.0$–0.075. The inset is the best fit of Arrhenius plot in the range 300–200 K.

For thin film q is supposed to equal 3 for two dimensions hopping while it can be 4 for three dimensions hopping. $\sigma_{0\,\mathrm{Mott}}$ is given by Eq. (7)[37].

$$\sigma_{0\mathrm{Mott}} = \frac{3e^2 v}{(8\pi)^{1/2}} \left(\frac{\zeta N(E_F)}{k_B}\right)^{1/2} \tag{7}$$

And $T_{0\,\mathrm{Mott}}$ is as follows:

$$T_{0\mathrm{Mott}} = \frac{18}{k_B \xi^3 N(E_F)} \tag{8}$$

where $\sigma_{0\ \mathrm{Mott}}$ is hopping conductivity, v is phonon length, $T_{0\ \mathrm{Mott}}$ is characterized temperature depends on the density state on Fermi level $N(E_F)$ and ξ is localization length.

For sample with $x = 0.075$, it is interestingly found that it has best fitting and satisfy the conditions of Mott VRH for region II in the range 135–210 K. Fig. 7b shows the relation between $\mathrm{Ln}\sigma\ T^{1/2}$ and $T^{-1/3}$ is linear with fitness coefficient $R^2 = 0.9979$. The parameters of Mott variable hopping are given Table 3.

In order to verify the hopping condition, the hopping distance $R_{\mathrm{hop\,Mott}}$ and hopping energy $\Delta_{\mathrm{hop\,Mott}}$ has been calculated according to Eqs. (9) and (10) [37].

$$R_{\mathrm{hop\ Mott}}/\xi = \frac{3}{8}(T_{0\mathrm{Mott}}/T)^{1/4} \tag{9}$$

$$\Delta_{\mathrm{hop\ Mott}} = \frac{1}{4} k_B T (T_{0\mathrm{Mott}}/T)^{1/4} \tag{10}$$

It can be noticed that the localize length ξ_{Mott} is in the order of nm and the ratio of hopping distance to localize length, $R_{\mathrm{hop\,Mott}}/\xi_{\mathrm{Mott}} > 1$ nm. This condition is satisfying the hopping condition of the system [38].

At lower temperature, in the range 85–130 K, the conducting mechanism for all samples is found to follow VRH ES, Fig. 8. The conductivity in VRH ES model is given by Eq. (11) [39].

$$\sigma_{\mathrm{VRH\ ES}} = \sigma_{0\mathrm{ES}} T^{-1} \exp\left(-T_{0\mathrm{ES}}/T\right)^{1/2} \tag{11}$$

where $T_{0\,\mathrm{ES}}$ is given by

$$T_{0\mathrm{ES}} = \frac{2.8e^2}{k_B \xi \varepsilon} \tag{12}$$

where $T_{0\,\mathrm{ES}}$ is characteristic temperature and $\sigma_{\mathrm{VRH\ ES}}$ hopping conductivity. The hopping parameters are listed in Table 4. The hopping distance $R_{\mathrm{hop\ ES}}$ and hopping energy $\Delta_{\mathrm{hop\ ES}}$ are calculated from Eqs. (13) and (14) [39].

Table 2
Thermal activation conduction band E_{a1}, temperature range, fitting coefficient R^2, Thermionic emission via grain boundary E_b and thermal activated hopping E_{a2} of thin films.

	Thermal activated conduction band		Thermionic emission via grain boundary			Thermal activated hopping	
	Temperature range/fitting coefficient, R^2	Thermal activation energy E_{a1} (meV)	L_D (nm)	N_d (cm^{-3})	E_b (meV)	Temperature range/fitting R^2	E_{a2} (meV)
$X = 0$	300–210 K/0.9995	66.8	1.15	9.7×10^{18}	77	140–210 K/0.9953	38
$X = 0.025$	300–195 K/0.9978	43.8	1.52	5.5×10^{18}	53.6	135–190 K/0.9968	28
$X = 0.05$	300–215 K/0.9991	41	2.6	1.9×10^{18}	51.4	130–210 K/0.995	26.3
$X = 0.075$	300–220 K/0.9967	35	3	1.4×10^{18}	45.8	_	_

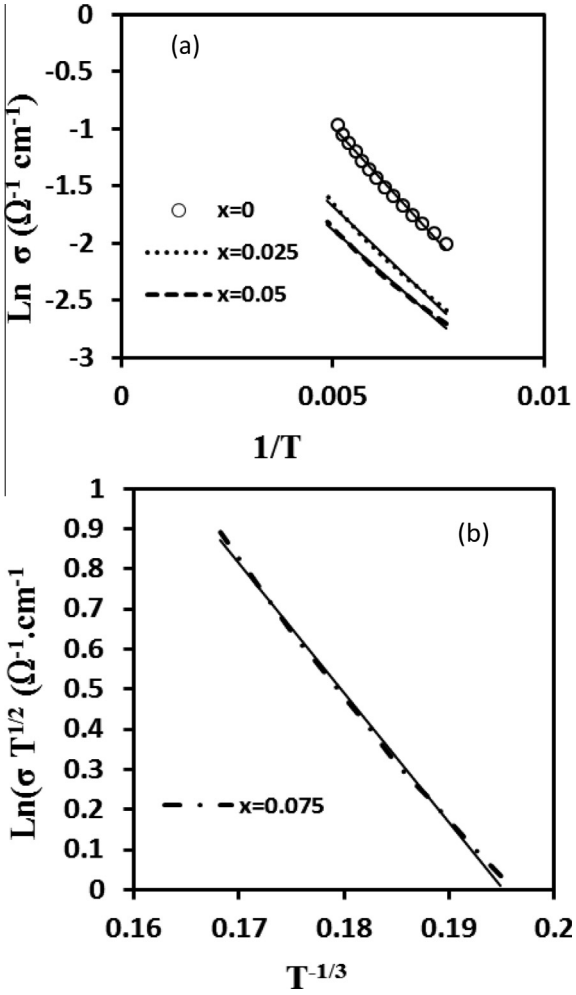

Fig. 7. (a) Lnσ against T^{-1} of thin films with $x = 0.0$–0.05. (b) Lnσ $T^{1/2}$ against $T^{-1/3}$ of thin film with $x = 0.075$.

$$R_{\text{hop ES}}/\xi = \frac{1}{4}(T_{0\text{ES}}/T)^{1/2} \tag{13}$$

$$\Delta_{\text{hop ES}} = \frac{1}{2}k_B T(T_{0\text{ES}}/T)^{1/2} \tag{14}$$

The localize length ξ is in the order of nm while $R_{\text{hop ES}}/\xi_{\text{ES}} \geqslant 1$. These conditions are fulfilled the hopping conditions [38]. The increment of Cr concentration in In_2O_3 system reduces the hopping energy but increases the hopping distance and localize length, which result in reducing the hopping conductivity and characteristic temperature $T_{0\,\text{ES}}$. The VRH ES mechanism has been also observed at low temperature $T < 100$ K for SnO_2 thin film prepared by sol–gel spin coating method [32].

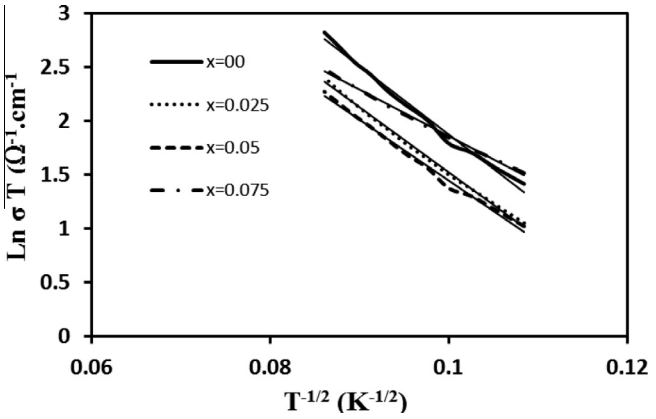

Fig. 8. Lnσ T against $T^{-1/2}$ in the range 85–130 K, the solids are best with best fitting.

3.5. Optical properties of Cr doped In_2O_3

The optical transmission of undoped and chromium doped indium oxide is shown in Fig. 9a. The transmission is over 90% for all samples. Since the samples have different thickness, the absorption coefficient vs wavelength has been plotted in order makes a better optical properties comparison between the sample (Fig. 9b). It can be observed that the absorption above 560 nm decreases with the increment of Cr dopant up to $x = 0.05$ then decreases for $x = 0.075$. Table 5 presents a comparison between current results with other transparent thin film systems such as Al doped ZnO (AZO), Ga doped ZnO (GZO) and Sn doped In_2O_3 (ITO). It shows that our film with $x = 0.05$ has highest transmission over all films and resistivity lower than GZO film however it has higher resistivity than ITO and AZO.

The relation between absorption coefficient and energy band gap can be given by the following Eq. (14),

$$(\alpha h\nu)^n = (h\nu - E_g) \tag{15}$$

where α is the absorption coefficient, $h\nu$ is the photon energy, and Eg is the energy band gap. n is a constant equal to 2, 2/3, 1/2, 1/3 for allowed direct, forbidden indirect, allowed indirect, forbidden indirect transitions, respectively. Band gap was estimated from the relation between $(\alpha h\nu)^2$ vs $h\nu$, see Fig. 10. This relation

Table 3
Temperature range, fitting coef. Characteristic temperature $T_{0\,\text{Mott}}$, hopping conductivity $\sigma_{0\,\text{Mott}}$, localize hopping ξ_{Mott}, density state $N(E_F)$, hopping distance $R_{\text{hop Mott}}$, hopping energy Δ_{hop} and $R_{\text{hop}}/\xi_{\text{Mott}}$ of thin film with $x = 0.075$.

Temp. range/linear fitting R^2	$T_{0\,\text{Mott}}$ (K)	$\sigma_{0\,\text{Mott}}$ (Ω^{-1} cm^{-1})	ξ_{Mott} (nm)	$N(E_F)$ (eV cm^{-3})	$R_{\text{hop Mott}}$ (nm)	Δ_{hop} (meV)	$R_{\text{hop}}/\xi_{\text{Mott}}$
135–210 K/0.9979	1075037	492.7	1.86	3×10^{19}	6.4	29	3.45

Table 4
Temperature range, linear fitting coefficient R^2, characteristic temperature $T_{0\,ES}$, hopping conductivity $\sigma_{0\,ES}$, localize hopping ξ_{ES}, distance hopping $R_{hop\,ES}$, hopping energy Δ_{hop} and $R_{hop\,ES}/\xi_{ES}$.

	Temp. range /linear fitting coefficient, R^2	$T_{0\,ES}$ (K)	$\sigma_{0\,ES}$ (Ω^{-1} cm^{-1})	ξ_{ES} (nm)	$R_{hop\,ES}$ (nm)	Δ_{hop} (meV)	R_{hop}/ξ_{ES}
x = 00	85–135 K/0.9903	3844	2981	1.35	2.2	25	1.63
x = 0.025	85–130 K/0.9945	3226	1339	1.6	2.4	23	1.5
x = 0.05	85–130 K/0.9929	3080	1096	1.7	2.5	22	1.46
x = 0.075	80–135 K/0.9943	1722	403	3	3.3	17	1.1

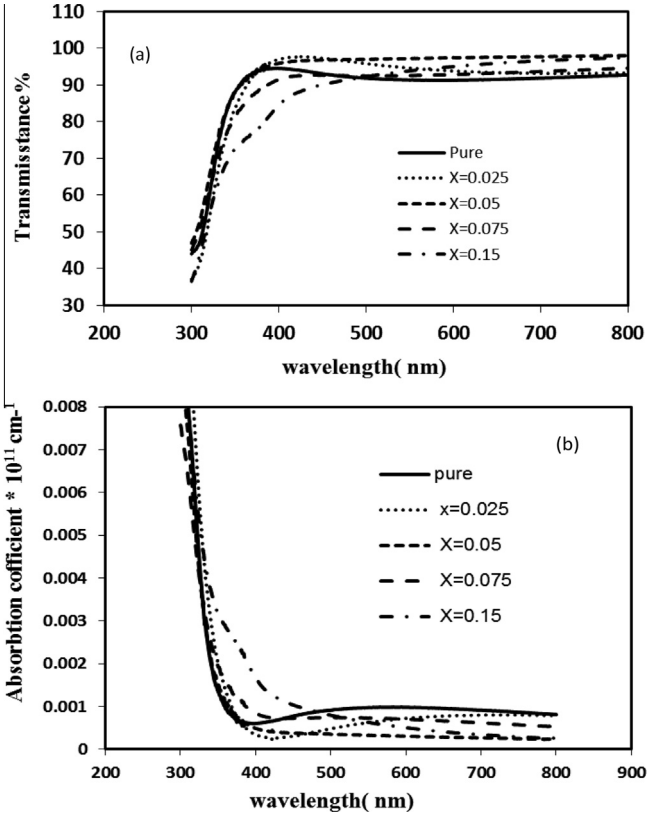

Fig. 9. Optical transmission (a) and (b) absorption coefficient of $In_{2-x}Cr_xO_3$ thin films.

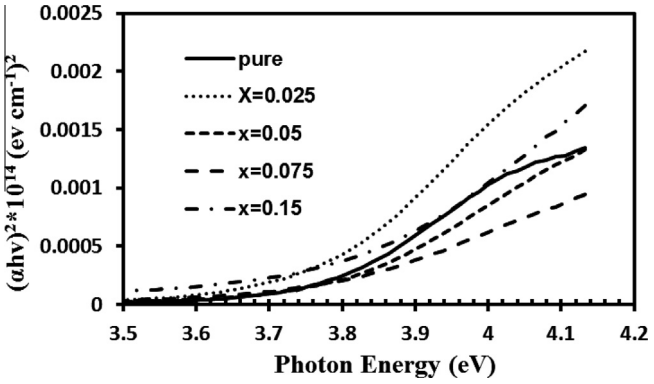

Fig. 10. Plot of $(\alpha h\nu)^2$ against $h\nu$ of $In_{2-x}Cr_xO_3$ thin films.

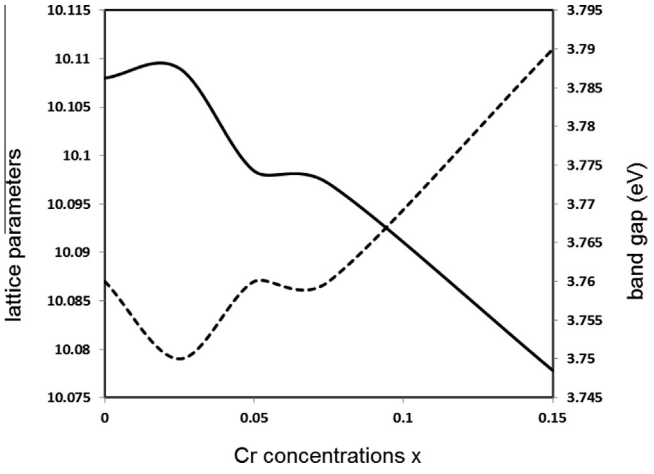

Fig. 11. Lattice parameter a and band gap vs Cr (bold line for lattice parameter and dot line for band gap).

is parabolic curve and band gap was estimated by extrapolation straight line to the linear part to intersect $h\nu$ axis at E_g value. In our calculation, n was fixed to 2 because the extrapolation line has maximum fitness with curves at n equal 2.

The band gap for pure sample is 3.76 eV. This result was also reported by [43] for (2 2 2) oriented indium oxide thin film deposited on MgO (1 0 0) substrate by metal organic chemical vapour deposition (MOCVD). The band gaps of $In_{2-x}Cr_xO_3$ films have a little change for low dopant $x \leqslant 0.075$, however it increases at maximum Cr concentration, x = 0.15, as summarized in Table. 1. The electrical measurement indicates that Cr dopant doesn't provide carrier (electrons) in In_2O_3 but decrease the carrier concentration gradually. So the widening of band gap doesn't follow Burstein–Moss (BM) shift for doped semiconductors associated with the increment of carrier concentration. This is in good agreement with a report in the literature. Caricato et al. have reported that the low Cr concentration in ITO narrows the band gap, however for high Cr concentration, the band gap is widening [44]. The doping of Cr at

Table 5
The electrical and transmission properties comparison between current study with AZO, GZO and ITO.

TCO Thin film	Resistivity (Ω cm),	Carrier concentration cm^{-3}	Mobility	Transmission at 800 nm	Ref.
In_2O_3	0.29	9.8×10^{18}	2.16	93	Current
$In_{1.95}Cr_{0.05}O_3$	3.5	1.9×10^{18}	1.43	98	Current
AZO (Al 2%)	~0.2	9×10^{18}	12	~85	[40]
GZO (Ga 2%)	~200	–	–	~91	[41]
ITO	~0.013–0.006	~$(1.4–1.8) \times 10^{20}$	~3.1–6	~92–94	[42]

Note: Samples from Refs. [40–42] were prepared using a sol–gel method and annealed at 500 °C.

a high concentration could lead to disorder in crystal symmetry by shrinking the lattice parameters which leads to the reconstruction of band structure, thus widen the band gap (the relation between lattice parameter, a and band gap vs Cr concentrations is shown in Fig. 11). On the other hand the relations between carrier concentration and band gap values is consistent with results reported for Cr-doped indium oxide prepared on Si substrate by rf sputtering at room temperature [20]. The carrier concentrations of annealed films are 7.8×10^{20} cm^{-3} and the band gap value is 3.63 eV. After heat treatment the carrier concentration is 2.0×10^{20} cm^{-3} and energy gap is 3.89 eV [20].

4. Conclusion

High quality In_2O_3 and Cr-doped In_2O_3 ($In_{2-x}Cr_xO_3$) nanocrystals thin films have been prepared by a simple sol–gel method followed spin coating technique. All films have single phase In_2O_3 structure and no traces of secondary phase related to Cr or its compound has been detected. The lattice parameter, of In_2O_3 system increased at lowest dopants ($x = 0.025$) and decreases with the increment of dopants. In_2O_3 has 92% transmittance with resistivity, mobility and band gap of 0.29 Ω cm, 2.1 cm^2 V^{-1} S^{-1} and 3.76 eV, respectively. The optical transmittance increased with the increment of Cr doping concentration up to 98% for $x = 0.05$. The Cr dopant strongly affects the microstructure of In_2O_3 system. The sample's surface has spherical agglomerated particle at $x = 0.025$–0.05. For samples with $x \geqslant 0.075$ the films surfaces become porous which increased with further doping. At $x = 0.15$ the grains connect to each and form flower like microstructure. The root mean square roughness ranges from 1.755 nm for sample with $x = 0.025$ to 7 nm for sample with $x = 0.15$ and it is varied with dependence to the agglomeration of grains and porosity of the sample's surface. The band gap values show little change at low Cr concentration $x \leqslant 0.075$ and increased at $x = 0.15$. The grain boundary affected the conduction in the range 300–200 K and its thermionic emission energy decreased with the increment of Cr dopant. The electrical conduction in the range 210–140 K was characteristic by nearest–nearest hopping conduction at $x = 00$–0.05 and by Mott variable hopping at $x = 0.075$. Efros–Shklovskii variable range hopping is found to dominant in the range 85–130 K for all samples. In_2O_3 and Cr doped In_2O_3 compound can be used as sensors and in transparent oxide applications.

Acknowledgement

This work was supported by Malaysian Ministry of Science and Technology via Grant Nos. 03-01-02-SF0742 and UKM-OUP-FST-2012.

References

[1] V. Shelke, M.P. Bhole, D.S. Patil, Solid State Sciences 14 (2012) 705–710.
[2] V. Shelke, M.P. Bhole, D.S. Patil, Journal of Alloys and Compounds 560 (2013) 147–150.
[3] V. Shelke, B.K. Sonawane, M.P. Bhole, D.S. Patil, Journal of Non-Crystalline Solids 355 (2009) 840–843.
[4] V. Shelke, B.K. Sonawane, M.P. Bhole, D.S. Patil, Journal of Materials Science: Materials in Electronics 23 (2012) 451–456.
[5] B.K. Sonawane, V. Shelke, M.P. Bhole, D.S. Patil, Journal of Physics and Chemistry of Solids 72 (2011) 1442–1446.
[6] B.K. Sonawane, M.P. Bhole, D.S. Patil, Optical and Quantum Electronics 41 (2009) 17–26.
[7] M. Yang, J. Feng, G. Li, Q. Zhang, Journal of Crystal Growth 310 (2008) 3474–3477.
[8] N. Manavizadeh, F.A. Boroumand, E. Asl-Soleimani, F. Raissi, S. Bagherzadeh, A. Khodayari, M.A. Rasouli, Thin Solid Films 517 (2009) 2324–2327.
[9] Z.-H. Li, E.S. Cho, S.J. Kwon, Applied Surface Science 257 (2010) 776–780.
[10] R.K. Gupta, K. Ghosh, S.R. Mishra, P.K. Kahol, Applied Surface Science 254 (2008) 4018–4023.
[11] C. Shekhar, K.I. Gnanasekar, E. Prabhu, V. Jayaraman, T. Gnanasekaran, Sensors and Actuators B: Chemical 155 (2011) 19–27.
[12] M.P. Bole, D.S. Patil, Journal of Physics and Chemistry of Solids 70 (2009) 466–471.
[13] D.-W. Kang, S.-H. Kuk, K.-S. Ji, H.-M. Lee, M.-K. Han, Solar Energy Materials and Solar Cells 95 (2011) 138–141.
[14] D. Antonia Sonia Alves Cardoso, Renewable Energy 36 (2011) 1153–1165.
[15] D.J. Payne, E.A. Marquis, Chemistry of Materials 23 (2011) 1085–1087.
[16] G.Z. Xing, J.B. Yi, D.D. Wang, L. Liao, T. Yu, Z.X. Shen, C.H.A. Huan, T.C. Sum, J. Ding, T. Wu, Physical Review B 79 (2009) 174406.
[17] F.-X. Jiang, X.-H. Xu, J. Zhang, X.-C. Fan, H.-S. Wu, G.A. Gehring, Applied Physics Letters 96 (2010) 052503.
[18] P. Kharel, C. Sudakar, M.B. Sahana, G. Lawes, R. Suryanarayanan, R. Naik, V.M. Naik, Journal of Applied Physics 101 (2007). 09H117-109H117-113.
[19] J. Philip, A. Punnoose, B.I. Kim, K.M. Reddy, S. Layne, J.O. Holmes, B. Satpati, P.R. LeClair, T.S. Santos, J.S. Moodera, Nature Materials 5 (2006) 298–304.
[20] C.Y. Hsu, Thin Solid Films 520 (2012) 2311–2315.
[21] N.B. Ukah, R.K. Gupta, P.K. Kahol, K. Ghosh, Applied Surface Science 255 (2009) 9420–9424.
[22] R. Shaiboub, N.B. Ibrahim, M. Abdullah, F. Abdulhade, Journal of Nanomaterials 2012 (2012) 1–5.
[23] H.Z. Chen, M.C. Kao, S.L. Young, C.C. Yu, C.H. Lin, C.M. Lee, C.R. Ou, Thin Solid Films 517 (2009) 4818–4821.
[24] F. Aldbea, N.B. Ibrahim, M. Abdullah, R. Shaiboub, Journal of Sol–Gel Science and Technology 62 (2012) 483–489.
[25] A. Bourlange, D.J. Payne, R.G. Palgrave, H. Zhang, J.S. Foord, R.G. Egdell, R.M.J. Jacobs, T.D. Veal, P.D.C. King, C.F. McConville, Journal of Applied Physics 106 (2009) 013703–013709.
[26] Y. Shigesato, Y. Hayashi, T. Haranoh, Applied Physics Letters 61 (1992) 73–75.
[27] J. Popović, E. Tkalčec, B. Gržeta, C. Goebbert, V. Ksenofontov, M. Takeda, Zeitschrift für Kristallographie Supplements 2007 (2007) 489–494.
[28] M.A. Flores-Mendoza, R. Castanedo-Perez, G. Torres-Delgado, J. Márquez Marín, O. Zelaya-Angel, Thin Solid Films 517 (2008) 681–685.
[29] T. Tomita, K. Yamashita, Y. Hayafuji, H. Adachi, Applied Physics Letters 87 (2005) 051911–051913.
[30] J. Mazloom, F.E. Ghodsi, Materials Research Bulletin 48 (2013) 1468–1476.
[31] J. Han, M. Shen, W. Cao, A.M.R. Senos, P.Q. Mantas, Applied Physics Letters 82 (2003) 67–69.
[32] N. Serin, A. Yildiz, A.A. Alsaç, T. Serin, Thin Solid Films 519 (2011) 2302–2307.
[33] S.K. Neogi, R. Ghosh, G.K. Paul, S.K. Bera, S. Bandyopadhyay, Journal of Alloys and Compounds 487 (2009) 269–273.
[34] R. Kumar, N. Khare, Thin Solid Films 516 (2008) 1302–1307.
[35] V.F. Gantmakher, Electrons and Disorder in Solids, Oxford University Press, New York, 2005.
[36] J.W. Orton, M.J. Powell, Reports on Progress in Physics 43 (1980) 1263.
[37] E.A. Davis, N.F. Mott, Electronic Properties in Non-Crystalline Materials, Clarendon Press, Oxford, 1971.
[38] A. Yildiz, S.B. Lisesivdin, M. Kasap, D. Mardare, Journal of Non-Crystalline Solids 354 (2008) 4944–4947.
[39] A.L. Efros, B.I. Shklovskii, Electronic Properties of Doped Semiconductors, Springer, Berlin, 1984.
[40] K.E. Lee, M. Wang, E.J. Kim, S.H. Hahn, Current Applied Physics 9 (2009) 683–687.
[41] C.-Y. Tsay, K.-S. Fan, C.-M. Lei, Journal of Alloys and Compounds 512 (2012) 216–222.
[42] C.-C. Ting, W.-L. Cheng, G.-C. Lin, Thin Solid Films 519 (2011) 4286–4292.
[43] L. Kong, J. Ma, C. Luan, Z. Zhu, Q. Yu, Surface Science 605 (2011) 977–981.
[44] A. Caricato, M. Cesaria, A. Luches, M. Martino, G. Maruccio, D. Valerini, M. Catalano, A. Cola, M. Manera, M. Lomascolo, A. Taurino, R. Rella, Applied Physics A: Materials Science & Processing 101 (2010) 753–758.